Chemical Physics Letters 455 (2008) 242–248

Contents lists available at ScienceDirect

Chemical Physics Letters

journal homepage: www.elsevier.com/locate/cplett

Impedance of carrier injection at the metal–organic interface mediated by surface states in electron-only tris(8-hydroxyquinoline) aluminium (Alq_3) thin layers

Germà Garcia-Belmonte [a,*], Juan Bisquert [a], Paulo R. Bueno [b], C.F.O. Graeff [c]

[a] Departament de Física, Universitat Jaume I, E-12071 Castelló, Spain
[b] Universidade Estadual Paulista, Instituto de Química, C. Postal 355, CEP 14800-900, Araraquara - SP, Brazil
[c] Departamento de Física, Faculdade de Ciências, UNESP, Av. Luiz Edmundo Carrijo Coube 14-01, 17033-360 Bauru, Brazil

ARTICLE INFO

Article history:
Received 9 January 2008
In final form 23 February 2008
Available online 29 February 2008

ABSTRACT

Capacitance spectra of thin (<200 nm) Alq_3 electron-only devices have been measured as a function of bias voltage. Capacitance spectra exhibit a flat response at high frequencies (>10^3 Hz) and no feature related to the carrier transit time is observed. Toward low frequencies the spectra reach a maximum and develop a negative excess capacitance. Capacitance response along with current–voltage (*J*–*V*) characteristics are interpreted in terms of the injection of electrons mediated by surface states at the metal–organic interface. A detailed model for the impedance of the injection process is provided that highlights the role of the filling/releasing kinetics of energetically distributed interface states. This approach connects the whole capacitance spectra to the occupancy of interface states, with no additional information about bulk trap levels. Simulations based on the model allow to derive the density of interface states effectively intervening in the carrier injection ($\sim 1.5 \times 10^{12}$ cm^{-2}).

© 2008 Elsevier B.V. All rights reserved.

1. Introduction

Interfaces between metals and organic semiconductors constitute a determining part of organic electronics [1]. A fundamental knowledge of the mechanisms underlying charge carrier injection from a metal into an organic semiconductor as well as bulk transport characteristics are essential to design efficient devices. In the specific case of organic light-emitting diodes (OLEDs), a framework able to predict the injection of charge carriers (particularly electrons) at interfaces between metals and organic semiconductors remains elusive despite the important amount of experimental data and proposed theoretical approaches that are available [2–7]. Reported experimental data show results that appear to be contradictory when comparing the response of similar devices prepared in different laboratories. It is then a crucial issue to reveal which preparing conditions or device structure give rise to particular current-limiting mechanisms.

For the archetypical electron-transporting and luminescent compound tris(8-hydroxyquinoline) aluminium (Alq_3) there exist in the literature sound evidences which relate the device current to either space-charge limited transport or interface-limited injection. The *J*–*V* characteristics of Alq_3-based devices, which seldom exhibit the behavior $J \propto V^m$ with $m > 2$, have been interpreted in terms of trap-charge limited conduction with the parameter $m - 1 = E_t/k_BT$ being related to the characteristic energy of the exponential trap tail E_t [8,9]. Such analysis has been improved by regarding the dependence of the mobility on temperature and electrical filed F as $\mu = \mu_0 \exp(\beta\sqrt{F})$ [10–12]. The Gaussian density-of-states (DOS) corresponding to the lowest unoccupied molecular orbital (LUMO) levels was also invoked [13] to account for the *J*–*V* characteristics of Al/Alq_3/LiF/Al devices at room-temperature in a trap-free explanation. On the other hand, injection limited *J*–*V* characteristics were proposed for structures of the type Al/Alq_3/Mg:Ag with injection barrier of 0.5 eV [5] and 0.6 eV in the case of the structure Ca/Alq_3/Ca [14]. Charge-carrier injection at metal–organic interfaces has been analyzed in terms of the diffusion-limited thermionic emission [15]. This approach has been improved by considering the injection into an energetically disordered organic solid as a sequential process in which carriers hop from the metal Fermi level to localized states, exhibiting Gaussian energy disorder, close to the interface [2,16]. It has been further recognized that such approach is unable to yield the usually observed power-law relationship $J \propto V^m$ [6]. Instead of considering the first hop from the metal Fermi level into the organic film as the energetically costly event, Baldo and Forrest [6] developed an injection model which considers the determining role of intermediate states induced by interface dipoles. This last approach is in agreement with the observed power-law *J*–*V* characteristics, and it was validated for different Alq_3 structures (with LiF/Al, Mg:Ag, and Al cathodes) of thickness <200 nm.

* Corresponding author. Fax: +34 964 729218.
E-mail address: garciag@uji.es (G. Garcia-Belmonte).

0009-2614/$ - see front matter © 2008 Elsevier B.V. All rights reserved.
doi:10.1016/j.cplett.2008.02.076

Apart from checking the model validity by varying a series of external parameters such as active layer thickness, temperature and metal contacts [11], the investigation of dynamic or transient properties (i.e. impedance response) might provide new insights and help selection of the device model. Whereas the sole analysis of steady-state *J–V* characteristics appear to be non-definitive in most cases, frequency- or time-resolved techniques could be determinant by revealing exclusive spectroscopic patterns. In this sense the work by Berleb and Brütting [17] on Al/Alq_3/Ca electron-only devices clearly demonstrated the space-charge limited origin of the capacitance spectra. A minimum is observed in $C(\omega)$ (kneelike feature of about 5% reduction) which is related to the electron transit time τ_t and allows to determine the carrier mobility μ_e. For Alq_3 samples with thickness longer than 200 nm experimental data from different techniques were then consistent with a unique device model: current is space-charge limited (including trap states) by dispersive transport of electrons. However, such clear picture is not complete for thinner films (<200 nm). As Brütting pointed out [11] films with 100 nm-thickness exhibited *J–V* characteristics that did not match those predicted using values extracted from the analysis of thicker structures. Although *J–V* characteristics followed the expected behavior $J \propto V^m$ for space-charge limited current (SCLC) with traps, the influence of some type of injection-limitation was recognized [11]. In addition to well-known ac expressions for SCLC, impedance models for electron-injection based on a sequential hopping process have been recently proposed [18].

The aim of this work was to verify whether SCLC trends are still observable in thin (<200 nm) Alq_3 electron-only devices when frequency-resolved techniques such as impedance spectroscopy are used. In particular we observed that the characteristic frequency related to the transit time is not present in the measured capacitance spectra. At higher bias the response changes to an inductive behavior, clearly visible as the negative values reached by the capacitance at low frequencies. Such negative capacitance response has been reported by many authors [18–21]. These two trends, namely the absence of SCLC features and the negative values at low frequencies in the capacitance spectra, have been interpreted as strong indication of the injection-limited mechanism underlying the device operation. The paper is structured as follows: in Section 2 experimental results (*J–V* characteristics and capacitance spectra) are presented. It is explained how purely bulk models have difficulty interpreting the experimental results. Consequently, an electron-injection model able to simultaneously account for both steady-state and dynamic responses is described with high degree of generality in Section 3. Finally, Section 4 is devoted to the comparison between the experimental results in Section 2 and model simulations.

2. Experimental results

The devices used in this study had the following structure Al/LiF(0.8 nm)/Alq_3(150 nm)/LiF(0.8 nm)/Al, where the number in parentheses indicate the layer thickness. Alq_3 was purified by gradient sublimation and evaporated at a rate of 1.0 Å/s. Lithium Fluoride (LiF) was deposited at a rate of 0.2 Å/s. Both LiF and Alq_3 layers were thermally evaporated at a base pressure of around 5×10^{-7} mbar during the same fabrication process, without breaking the vacuum. Al electrodes (100 nm) were deposited in another chamber at a rate of 11 Å/s, at a pressure of around 2×10^{-6} mbar, to form device active areas of 4 mm^2. For the measurements, devices were encapsulated in nitrogen atmosphere inside quartz tubes. Impedance measurements were performed using a Solartron 1260 frequency response analyzer (FRA). A dielectric interface (SI 1296) was coupled to the FRA in order to achieve higher sensitivity in the high impedance dielectric range. Oscillating amplitude of 10 mV was added to the dc bias voltage using frequencies within the range of 1 MHz down to 0.1 Hz. Capacitance spectra were obtained from the impedance Z as $C = Re(1/i\omega Z)$, where $i = \sqrt{-1}$ and ω is the angular frequency of the ac perturbation.

The *J–V* characteristics of a L = 150 nm-thick Al/LiF/Alq_3/LiF/Al device measured at room temperature is shown in Fig. 1. The current density obtained lies within the range of that reported for similar devices [11]. As expected the device exhibits symmetrical characteristics with a power-law exponent ($m \approx 5.4$) in $J \propto V^m$. Instead of following the experimental procedure of varying temperature and sample thickness in order to discern the proper model (bulk or injection mechanism) accounting for such *J–V* characteristics, we adopt the approach of investigating the capacitance response under variation of the applied bias. By examining Fig. 2 one can realize that the capacitance is constant and bias-independent at high-frequencies (>10^3 Hz). This extremely flat response of C_0 = 0.70 nF corresponds to the geometrical capacitance of the device and yields a permittivity of ε = 2.96, typical for amorphous organic semiconductors. For low bias voltages (1 V) the capacitance grows monotonously toward lower frequencies. This feature has been usually interpreted in terms of trapping [22]. At higher bias the capacitance values reach a maximum at intermediate frequencies (1–10 Hz) and develop an inductive behavior in the low–

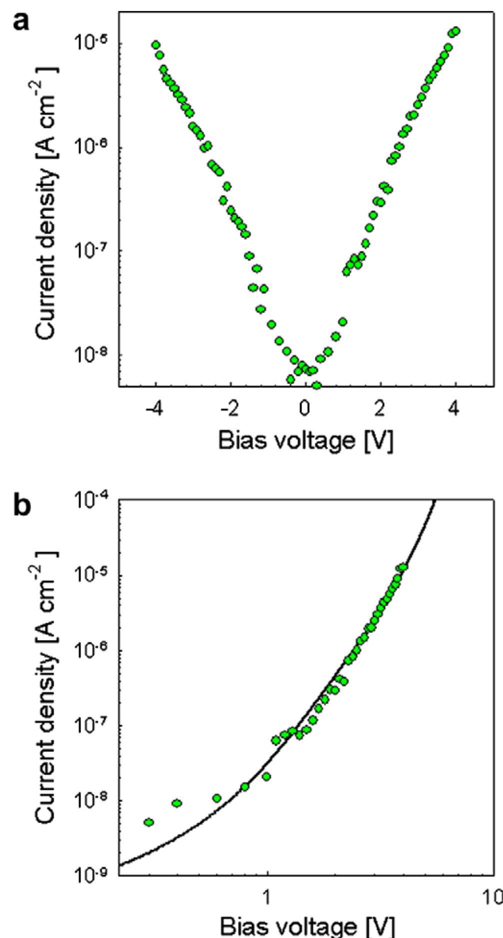

Fig. 1. *J–V* characteristics of a L = 150 nm-thick Al/LiF/Alq_3/LiF/Al device measured at room temperature. (a) Symmetrical response. (b) Comparison between experiment (dots) and electron-injection model prediction (solid line) in a log–log representation. Model parameters: N_I= 2.6×10^{15} cm^{-2}, N_B = 10^{20} cm^{-3}, E_{F0} = 0.0 eV, $E_2^r = 6$ eV, k_BT_0 = 0.7 eV, $E_3^r = 0.3$ eV, σ_B = 0.1 eV, α_1 = 1, α_2 = 0.065, k_{12} = 1 s^{-1}, $k_{23}N_B$ = 10^{-1} s^{-1}, γ_1 = 0.1, and γ_2 = 0.

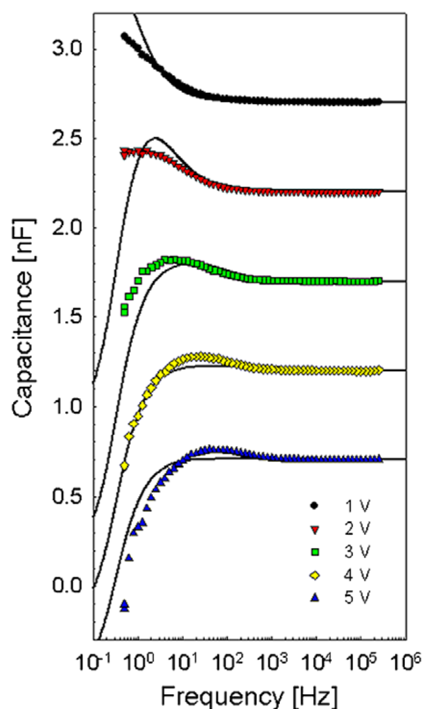

Fig. 2. Capacitance spectra of a L = 150 nm-thick Al/LiF/Alq_3/LiF/Al device measured at room temperature. Comparison between experiment (dots) and electron-injection model prediction (solid line) for different bias voltages. Same set of parameters as in Fig. 1. For the sake of clarity spectra are shifted 0.5 nF.

frequency limit. At 5 V-bias the negative contribution dominates and C becomes negative below 1 Hz.

One might try to interpret the measured capacitance spectra in terms of SCLC ac models [23]. The electron mobility of Alq_3 at room temperature [24] is known to be of the order of 10^{-6} cm^2/Vs what it would imply transit frequencies within the range of 1–100 kHz for bias of 1–5 V assuming relations like $\mu_e = 4L^2/3\tau_t F$ [25]. However, the small reduction in the capacitance values expected for SCLC at frequencies around the inverse of the transit time is not observed in any case. This experimental fact leads us to discard transport mechanism as responsible for the device operation, otherwise capacitance spectra should have shown SCLC features. It seems therefore that interface-limited injection can be behind the experimental observations in the line suggested by Baldo and Forrest [6].

The second distinctive feature of the capacitance spectra in Fig. 2 is the transition between positive to negative capacitance, as exhibited at high bias. Negative capacitance has been understood as originated from transport of minority carriers [26,27] or related to the electron–hole recombination [28], in both cases for double-injection devices. In the structures analyzed in this study the injection of holes is strongly blocked by effect of the LiF buffer layers, which reduces the barrier height for electron injection [29]. We can then discard recombination or hole conduction as the origin for the negative capacitance observed.

3. Electron-injection model

Recently we have proposed [18] a kinetic model based on simple assumptions about carrier injection at the device cathode able to reproduce the main features of the capacitive response: the exclusively positive capacitance response for hole-only devices, the collapse into a single pattern in the low bias region, and the shift toward lower bias of the inductive (negative capacitance) behavior for smaller work-function cathodes, in good correlation with experimental capacitance–voltage (C–V) curves [30]. We demonstrated [18] that the low-frequency (equilibrium) capacitance is proportional to the variation of the interfacial state occupancy with the bias voltage $C_c = qN_I\Delta\theta/\Delta V$ (q denotes the positive elementary charge, and θ is the occupancy of the interface states). The interface states are filled at low bias voltages so as to give increasing positive values of the low-frequency limit of the capacitance. At some point an increment in the applied bias promotes the intermediate state depopulation ($\Delta\theta < 0$) by a net flux of electrons injected into the LUMO of the bulk organic layer. The low-frequency limit of the capacitance then changes sign and becomes negative. Following this view the negative capacitance might be originated by a mechanism which is exclusively interfacial.

The model of carrier injection at the metal–organic interface has been detailed in previous publications [18,31] and is outlined in the diagram in Fig. 3. The injection from the metal Fermi level to the organic conductor LUMO (E_3) occurs sequentially, via interface states with energy E_2. In the previous papers [18,30,31], a single intermediate state was used. We first realized that such models were unable to reproduce the capacitance spectra shape observed in Fig. 2, in which the excess capacitance $\Delta C = C - C_0$ changes sign being positive at intermediate frequencies (~10 Hz) and developing a negative value at low frequencies. This led us to introduce distributions of states (DOS) into the calculation of the injection model. In the following, we present the derivation of the model using a distribution of states both in the dipole layer and in bulk

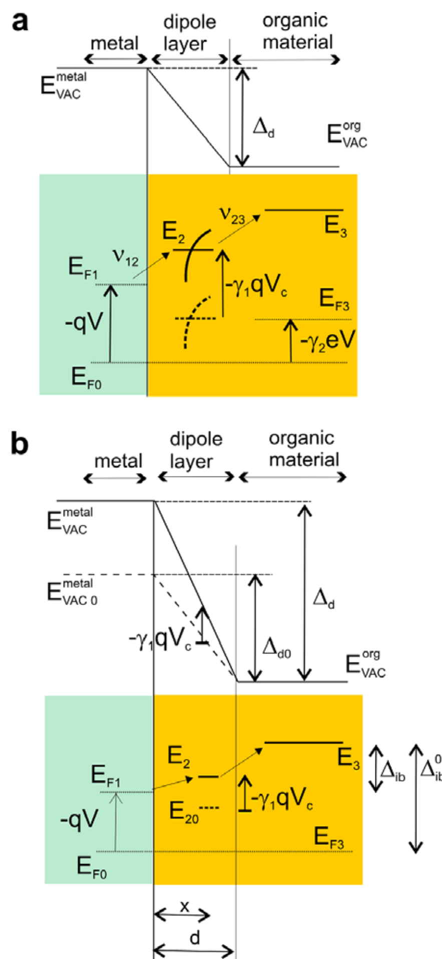

Fig. 3. Scheme of the injection model, showing the changes under applied negative bias potential. (a) Shift of the interfacial distribution, and change of the bulk carrier density. (b) Modification of the vacuum level discontinuity and the injection barrier.

levels of the organic material. A list of the symbols used is given in Table 1.

The applied potential is

$$V = -\frac{(E_{F1} - E_{F0})}{q} \tag{1}$$

One can define the potential at the cathode

$$V_c = -\frac{E_{F1} - E_{F3}}{q} \tag{2}$$

and the potential in the bulk

$$V_b = -\frac{E_{F3} - E_{F0}}{q} \tag{3}$$

so that

$$V = V_c + V_b \tag{4}$$

The occupation of the bulk levels at energy E_3 follows the Boltzmann function as

$$f(E_3, E_{F3}) = \exp\left[-(E_3 - E_{F3})/k_B T\right] \tag{5}$$

Therefore, the potential V_b determines the carrier density in the transport levels in proximity of the dipole layer. The change of occupation will have an effect on the injection model only at high carrier density, since it induces a return of injected charge from the bulk levels to the interfacial levels. For simplicity, we assume that the increase of carrier density in the bulk is determined by the parameter γ_2, according to the relationship

$$E_{F3} = E_{F0} + \gamma_2(E_{F1} - E_{F0}) \tag{6}$$

Table 1
List of symbols

Symbol	Meaning
q:	The positive elementary charge
k_BT:	The thermal energy
E_{F0}:	The equilibrium Fermi level
E_{F1}:	The Fermi level in the metal
E_{F3}:	The Fermi level in the bulk of the organic material
V:	The potential applied
V_c:	The potential applied in the cathode
V_b:	The potential applied in the bulk (increase of carrier density)
N_B:	The total density of states (per unit volume) in the bulk LUMO
E_2:	An interfacial level
E_{20}:	An interfacial level, at zero applied bias
E_2^r:	The reference interfacial level for the DOS
g_I:	The distribution of interfacial levels
E_3:	A level of the bulk LUMO in the organic conductor
E_{30}:	A level of the bulk LUMO, at zero applied bias
E_3^r:	A reference level for the distribution of the LUMO in the organic conductor
g_B:	The energy distribution of bulk levels
σ_B:	The Gaussian disorder of bulk levels
f:	The occupancy of bulk levels in the organic conductor
Δ_d:	The vacuum level discontinuity at the interface
Δ_{ib}:	The injection barrier
θ:	The occupancy of the interfacial level
N_I:	The total density (per unit area) of interfacial levels
T_0	The trap width parameter in interfacial levels
γ_1:	The parameter determining the shift of the interfacial levels under applied voltage
γ_2:	The parameter determining the increase of the bulk Fermi level under applied voltage
v_{12}:	The rate of transfer from metal to interfacial level
v_{23}:	The rate of transfer from interfacial to bulk levels
k_{12}:	The rate constant for transfer from metal to interfacial level
k_{23}:	The rate constant for transfer from interfacial to bulk level
α_1:	The asymmetry factor for transfer from metal to interfacial level
α_2:	The asymmetry factor for transfer from interfacial to bulk level
s:	Laplace variable
ω:	The angular frequency of the ac perturbation

Therefore, we obtain

$$V_c = (1 - \gamma_2)V \tag{7}$$

$$V_b = \gamma_2 V \tag{8}$$

In general, the increase of charge density in bulk levels will depend on the rapidity of evacuation of the carriers, i.e., the transport model, and also on the presence of opposite sign charge carriers. Therefore, this effect will be more significant in two-carrier devices, while in single carrier devices the density remains low and we can assume $\gamma_2 \approx 0$.

More significant for the injection model are the modifications under an applied potential occurring at the dipole layer, of width d, where the interface levels are located. In general, intermediate states are associated with the presence of interfacial dipoles. The gap states provide the charge required to establish thermodynamic equilibrium between the metal and the organic material, and it can be considered that the interfacial levels lie within the dipole layer [32,33]. In Fig. 3b, we assume that the interfacial levels lie a distance $x \leqslant d$ from the metal surface. In equilibrium, the net effect caused by the change of dipole energy at the interface is Δ_d^0 (the vacuum level discontinuity). A negative bias V_c increases $\Delta_d = \Delta_d^0 - qV_c$ and reduces the injection barrier $\Delta_{ib} = E_3 - E_{F1}$, as shown in Fig. 3b. The variation of Δ_d induces a shift of the interfacial levels. As indicated in Fig. 3b, the change of any energy level E_2 is

$$E_2 = E_{20} - q\frac{d - x}{d}V_c \tag{9}$$

We denote $\gamma_1 = 1 - x/d$. If $\gamma_1 \approx 1$ the energy level E_2 accompanies the variations of E_{F1}, and on the other hand, if $\gamma_1 \approx 0$, the interfacial level is pinned at the organic surface and remains stationary. From Eq. (9) we have

$$E_2 = E_{20} - q\gamma_1(1 - \gamma_2)V \tag{10}$$

Several forms of the DOS accounting for the interface level distribution were checked in order to reproduce the experimental data. At the end simulations match with capacitance and steady-state characteristics by assuming an exponential distribution for the interface levels, with respect to the reference level E_2^r

$$g_I(E_2^r - E_2) = \frac{N_I}{k_B T_0} \exp\left[-(E_2^r - E_2)/k_B T_0\right] \tag{11}$$

This distribution, shifts with the potential as indicated in Eq. (10) and depicted in Fig. 3a.

For the energy levels of the bulk organic material, we adopt a Gaussian distribution

$$g_B(E_3^r - E_3) = \frac{N_B}{\sqrt{2\pi}\sigma_B} \exp\left[-\frac{(E_3^r - E_3)^2}{2\sigma_B^2}\right] \tag{12}$$

as usually assumed as a consequence of fluctuations in polarization and dipole energies [34]. In most cases a value $\sigma_B \approx 0.1$ eV is found [35].

The rate of charge transfer *per site* between the metal and interfacial states at the energy E_2 is given by the expression [18]

$$v_{12}(E_2) = k_{12}\{(1 - \theta)A - \theta B\} \tag{13}$$

where

$$A = \exp\left[(\alpha_1 - 1)(E_2 - E_{F1})/k_B T\right] \tag{14}$$

$$B = \exp\left[\alpha_1(E_2 - E_{F1})/k_B T\right] \tag{15}$$

Similarly, the rate of charge transfer *per site* between the interface level and the bulk organic material is

$$v_{23}(E_2, E_3) = k_{23}\{\theta C - f(1 - \theta)D\} \tag{16}$$

where

$$C = \exp[\alpha_2(E_2 - E_3)/k_BT] \quad (17)$$

$$D = \exp[(\alpha_2 - 1)(E_2 - E_3)/k_BT] \quad (18)$$

The expression for the current density is

$$J(V) = q\int_{-\infty}^{+\infty} g_I(E_2, E_{20})v_{12}(E_2)\mathrm{d}E_2 \quad (19)$$

The rate of charge transfer from a E_2 level to bulk organic levels is

$$v_{23}(E_2) = k_{23}\int_{-\infty}^{+\infty} g_B(E_3, E_{30})\{\theta C - f(1-\theta)D\}\mathrm{d}E_3 \quad (20)$$

Therefore, we can write

$$v_{23}(E_2) = k_{23}\{\theta F - (1-\theta)G\} \quad (21)$$

where

$$F = \int_{-\infty}^{+\infty} g_B(E_3, E_{30})C\mathrm{d}E_3 \quad (22)$$

$$G = \int_{-\infty}^{+\infty} g_B(E_3, E_{30})fD\mathrm{d}E_3 \quad (23)$$

The change of the occupancy of the intermediate levels at the energy E_2 is given by

$$\frac{\mathrm{d}\theta(E_2)}{\mathrm{d}t} = v_{12}(E_2) - v_{23}(E_2) \quad (24)$$

At steady state, we can solve

$$v_{12}(E_2) - v_{23}(E_2) = 0 \quad (25)$$

and one readily obtains the occupancy of the level E_2

$$\theta(E_2) = \frac{1}{1 + \frac{B+bF}{A+bG}} \quad (26)$$

where

$$b = \frac{k_{23}}{k_{12}} \quad (27)$$

Inserting Eq. (26) in Eq. (19) we obtain the dc current. Note that the term in G in Eq. (26) corresponds to the return of charge from bulk levels to interfacial levels, and can normally be neglected.

Let us denote ac modulation of quantity y by Δy and the Laplace variable by $s = \mathrm{i}\omega$. The ac current is

$$\Delta J = q\int_{-\infty}^{+\infty} g_I(E_2^r - E_2)\left(\frac{\partial v_{12}}{\partial\theta}(E_2)\Delta\theta + \frac{\partial v_{12}}{\partial V}(E_2)\Delta V\right)\mathrm{d}E_2 \quad (28)$$

We obtain the admittance

$$Y = \frac{\Delta J}{\Delta V} = q\int_{-\infty}^{+\infty} g_I(E_2^r - E_2)\left(\frac{\partial v_{12}}{\partial\theta}(E_2)\frac{\Delta\theta}{\Delta V}(E_2) + \frac{\partial v_{12}}{\partial V}(E_2)\right)\mathrm{d}E_2 \quad (29)$$

The capacitance is defined as

$$C = \frac{Y}{s} \quad (30)$$

There remains to determine the term $\Delta\theta/\Delta V$ in Eq. (29). This is obtained from the kinetic Eq. (24) for the change of the occupancy of the intermediate level, that gives

$$s\Delta\theta(E_2) = \Delta v_{12}(E_2) - \Delta v_{23}(E_2) = \left\{\frac{\partial v_{12}}{\partial\theta}(E_2) - \frac{\partial v_{23}}{\partial\theta}(E_2)\right\}\Delta\theta + \left\{\frac{\partial v_{12}}{\partial V} - \frac{\partial v_{23}}{\partial V}\right\}\Delta V \quad (31)$$

Therefore

$$\frac{\Delta\theta}{\Delta V}(E_2) = \frac{\frac{\partial v_{12}}{\partial V}(E_2) - \frac{\partial v_{23}}{\partial V}(E_2)}{s - \frac{\partial v_{12}}{\partial\theta}(E_2) + \frac{\partial v_{23}}{\partial\theta}(E_2)} \quad (32)$$

By calculation, we find the partial derivatives that appear in Eqs. (29) and (32).

$$\frac{\partial v_{12}}{\partial\theta}(E_2) = -k_{12}(A+B) \quad (33)$$

$$\frac{\partial v_{12}}{\partial V}(E_2) = -\frac{q}{k_BT}k_{12}[1-\gamma_1(1-\gamma_2)]\{(1-\alpha_1)(1-\theta)A + \alpha_1\theta B\} \quad (34)$$

$$\frac{\partial v_{23}}{\partial\theta} = k_{23}(F+G) \quad (35)$$

$$\frac{\partial v_{23}}{\partial V} = -\frac{q}{k_BT}k_{23}\{\gamma_1(1-\gamma_2)\theta F + [(1-\alpha_2)\gamma_1(1-\gamma_2) - \gamma_2](1-\theta)G\} \quad (36)$$

This completes the model of the admittance.

4. Discussion

In the following we discuss on the parameters used in the simulation based on the described electron-injection model. We should emphasized that the model has to account for both steady-state and frequency-dependent characteristics with a single set of parameters giving a complete information of the charge injection process. The aim was to find a good enough reproduction of our particular experimental data, being conscious of the great amount of responses the parameters of the model could generate. Different forms of the interface DOS were carefully checked and the exponential distribution finally chosen. By examining Fig. 1b one can realize that the above outlined model [Eq. (19)] is able to reproduce with a good approximation the $J \propto V^m$ response for bias larger than 1 V. In this simulation the total interface DOS has been $N_I = 2.6 \times 10^{15}\ \mathrm{cm}^{-2}$, and total bulk density of $N_B = 10^{20}\ \mathrm{cm}^{-3}$ with $\sigma_B = 0.1$ eV. The interface state shift used in the simulation corresponds to $\gamma_1 = 0.1$, indicating that the intermediate levels are almost pinned at the organic surface. The effective density of occupied interface states can be calculated after considering the occupancy of each state and integration of Eq. (26). For bias of 5 V the effective interface DOS intervening in the injection process results $\sim 1.5 \times 10^{12}\ \mathrm{cm}^{-2}$, as observed in Fig. 4. It should be noted here that the order of magnitude obtained lies within typical values reported in the literature [6]. The intermediate state occupation reaches a maximum for levels located ~ 1.0 eV above the metal work function. These levels can be then interpreted as forming an *effective* electron energy barrier, which is highly determined by the injection kinetics. It has been recognized that metal–organic interfaces form structurally and chemically complex struc-

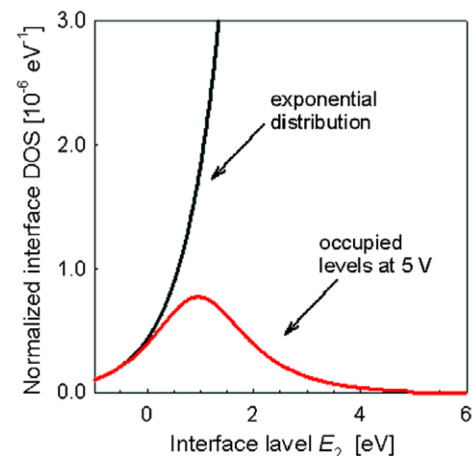

Fig. 4. Interface density-of-states following an exponential distribution (black) and portion of such states intervening in the injection process at 5 V of bias voltage. Same set of parameters as in Fig. 1.

tures. Diffusion and chemical reaction can lead to the formation of new metal–organic complexes with a different electronic structure than that observed in the bulk of the organic film [36]. The interfacial DOS characteristic energy $k_BT_0 = 0.7$ eV used in the simulation appears larger than the value deduced from purely bulk SCLC models (~0.1 eV). Other authors have discussed on the effect of the interface dipoles on the electron-energy distribution of the interface states with respect to the bulk DOS. Interfacial dipoles have been regarded to induce a broadening of 3–4 times the values encountered for bulk Gaussian DOS [6]. The energy difference between the cathode Fermi level and the LUMO levels used in the simulation was $E_3^r - E_{F0} = 0.3$ eV, which is a typical value and informs on the LiF layer effect on improving electron injection by increasing the dipole offset [37].

The asymmetry factors (transfer coefficients) [38] for electron transfer were chosen as $\alpha_1 = 1$ and $\alpha_2 = 0.065$. In case of $E_{F1} > E_2$ the first asymmetry factor reproduces transitions of the Miller–Abrahams type [39]. When $E_{F1} < E_2$ the back transition from intermediate states down to the metal is energetically favoured due to the positive overpotential as derived from Eqs. (14) and (15). Since $\alpha_2 \approx 0$ the second transitions ($2 \leftrightarrow 3$) are also governed by a mechanism similar to that encountered for $1 \leftrightarrow 2$, as one can see from Eqs. (17) and (18). It should be noted here that strict Miller–Abrahams-type transitions derive from hydrogenlike wave functions with spherical symmetry. It is then not surprising that hopping transition at the interface deviate from this simple form. The geometry of the Alq_3 molecule, with the three quinoline ligands pointing through different directions, or the special morphology of the LiF buffer layer might lay behind the values adopted for the asymmetry factors in the simulation.

Influence of the hopping rates is observed in the simulated capacitance spectra of Fig. 2, which result from Eqs. (29) and (30) plus the geometrical capacitance. A net rate constant k'_{23} for the second transitions from interfacial to bulk levels can be defined by integration of Eqs. (22) and (23). The total DOS of the bulk LUMO modifies the net rate as $k'_{23} = k_{23}N_B$. Since $k_{12} > k'_{23}$ ($k_{12} = 1\ \mathrm{s}^{-1}$, $k'_{23} = 10^{-1}\ \mathrm{s}^{-1}$) the effect of the interface state depopulation appears at lower frequencies, which allows the increment in the capacitance at intermediate frequencies related to the filling of interface states. Note here that the simulation captures the essential features of the experimental curves. For both experimental and simulated spectra, capacitance reaches a maximum with respect to the geometrical capacitance that slightly shifts toward high frequencies as the bias increases. In the low-frequency region the negative capacitance is reproduced. There is however slight differences between experimental and simulation curves that we tentatively attribute to possible dependences of the transition rate constants on the applied voltage. Positive values of the excess capacitance are previously proposed to derive from filling of bulk trap states [20,23]. Therefore, bulk models point to two different types of charge carriers to interpret the capacitance measurements. Whereas $\Delta C = C - C_0 < 0$ occurs as a consequence of reducing the amount of stored free carriers, $\Delta C > 0$ is believed to be related to the occupancy of traps. On the contrary, our approach simplifies the picture by seeing the evolution in the occupancy of interface states as responsible for the whole capacitance spectra change with bias. It must be stressed that some aspects remain unclear and need further work. Particularly, the observed slow kinetics of the filling/releasing process of interface states governing the carrier injection. This observation suggests us that not only the interface energetics plays a determining role in the injection process but also the kinetics of occupancy may have great influence for device modeling.

5. Conclusions

We have obtained a coherent picture about the processes governing thin (<200 nm) Alq_3 electron-only devices. Whereas J–V characteristics exhibiting $J \propto V^m$ behaviors might be interpreted either in terms of SCLC models or interface-limited injection, frequency-resolved techniques like impedance spectroscopy provide strong evidence which allows proper model selection. The fact that the capacitance spectra do not show the pattern predicted by SCLC theories leads us to see interface-limited injection as the determining mechanism for the device operation. Furthermore, negative values exhibited by the capacitance at high bias and low frequencies are in agreement with kinetic models of electron-injection through intermediate states. As a final conclusion we can say that deeper knowledge of the physico-chemical characteristics of such interface states and their relation to and influence of the dipole layer appears to be crucial.

Acknowledgement

We thank financial support from Ministerio de Educacion y Ciencia under project HOPE CSD2007-00007 (Consolider-Ingenio 2010) and Generalitat Valenciana under project ACOMP07/103. We acknowledge F. Nüesch and L. Zuppirolli for help in sample preparation as well as F. Castro for part of the measurements.

References

[1] Y. Shen, A.R. Hosseini, M.H. Wong, G.G. Malliaras, Chem. Phys. Phys. Chem. 5 (2004) 6.
[2] V.I. Arkhipov, E.V. Emelianova, Y.H. Tak, H. Bässler, J. Appl. Phys. 84 (1998) 848.
[3] V.I. Arkhipov, U. Wolf, H. Bässler, Phys. Rev. B 59 (1999) 7514.
[4] J.C. Scott, G.G. Malliaras, Chem. Phys. Lett. 299 (1999) 115.
[5] S. Barth et al., Phys. Rev. B 60 (1999) 8791.
[6] M.A. Baldo, S.R. Forrest, Phys. Rev. B 64 (2001) 085201.
[7] W.R. Silveira, J.A. Marohn, Phys. Rev. Lett. 93 (2004) 116104.
[8] P.E. Burrows, Z. Shen, V. Bulovic, D.M. McCarty, S.R. Forrest, J.A. Cronin, M.E. Thompson, J. Appl. Phys. 79 (1996) 7991.
[9] M. Stössel, J. Staudigel, F. Steuber, J. Blässing, J. Simmerer, Appl. Phys. Lett. 76 (2000) 115.
[10] S. Berleb, A.G. Mückl, W. Brütting, M. Schwoerer, Synth. Metal 111–112 (2000) 341.
[11] W. Brütting, S. Berleb, A.G. Mückl, Org. Electron. 2 (2001) 1.
[12] W. Brütting, S. Berleb, A.G. Mückl, Synth. Metal 122 (2001) 99.
[13] A. Ioannidis, E. Forsythe, Y. Gao, M.W. Wu, E.M. Conwell, Appl. Phys. Lett. 72 (1998) 3038.
[14] I.H. Campbell, D.L. Smith, Appl. Phys. Lett. 74 (1999) 561.
[15] P.R. Emtage, J.J. O'Dwyer, Phys. Rev. Lett. 16 (1966) 356.
[16] U. Wolf, V.I. Arkhipov, H. Bässler, Phys. Rev. B 59 (1999) 7507.
[17] S. Berleb, W. Brütting, Phys. Rev. Lett. 89 (2002) 286601.
[18] J. Bisquert, G. Garcia-Belmonte, A. Pitarch, H.J. Bolink, Chem. Phys. Lett. 422 (2006) 184.
[19] I.N. Hulea, R.F.J. van der Scheer, H.B. Brom, B.M.W. Langeveld-Voss, A. van Dijken, K. Brunner, Appl. Phys. Lett. 83 (2003) 1246.
[20] H.H.P. Gommans, M. Kemerink, G.G. Andersson, R.M.T. Pijper, Phys. Rev. B 69 (2004) 155216.
[21] F.A. Castro, P.R. Bueno, C.F.O. Graeff, F. Nüesch, L. Zuppiroli, L.F. Santos, R.M. Faria, Appl. Phys. Lett. 87 (2005) 013505.
[22] H.C.F. Martens, H.B. Brom, P.W.M. Blom, Phys. Rev. B 60 (1999) R8489.
[23] N.D. Nguyen, M. Schmeits, H.P. Loebl, Phys. Rev. B 75 (2007) 075307.
[24] R.G. Kepler, P.M. Beeson, S.J. Jacobs, R.A. Anderson, M.B. Sinclair, V.S. Valencia, P.A. Cahill, Appl. Phys. Lett. 66 (1995) 3618.
[25] M.A. Lampert, P. Mark, Current Injection in Solids, Academic Press, NY, 1970.
[26] H.H.P. Gommans, M. Kemerink, R.A.J. Janssen, Phys. Rev. B 72 (2005) 235204.
[27] M. Schmeits, J. Appl. Phys. 101 (2007) 084508.
[28] E. Ehrenfreund, C. Lungenschmied, G. Dennier, H. Neugebauer, N.S. Saricifti, Appl. Phys. Lett. 91 (2007) 012112.
[29] T. Mori, H. Fujikawa, S. Tokito, Y. Taga, Appl. Phys. Lett. 73 (1998) 2763.
[30] G. Garcia-Belmonte, H.J. Bolink, J. Bisquert, Phys. Rev. B 75 (2007) 085316.
[31] J. Bisquert, G. Garcia-Belmonte, J.M. Montero, H.J. Bolink, Proc. SPIE 6192 (2006) 619210.
[32] C. Shen, A. Kahn, Org. Electron. 2 (2001) 89.
[33] J.X. Tang, C.S. Lee, T.S. Lee, Y.B. Xu, Chem. Phys. Lett. 396 (2004) 92.

[34] R.H. Young, Philos. Mag. B 72 (1995) 435.
[35] J. Bisquert, G. Garcia-Belmonte, J. García-Cañadas, J. Chem. Phys. 120 (2004) 6726.
[36] C. Shen, A. Kahn, I. Hill, in: W.R. Salaneck, K. Seki, A. Kahn, J.-J. Pireaux (Eds.), Conjugated Polymer and Molecular Interfaces, first ed., Marcel Dekker, Inc., NY, 2002, p. 351.
[37] S. Tokito, H. Fujikawa, T. Mori, Y. Taga, in: W.R. Salaneck, K. Seki, A. Kahn, J.-J. Pireaux (Eds.), Conjugated Polymer and Molecular Interfaces, Marcel Dekker, Inc., NY, 2002, p. 525.
[38] A.J. Bard, L.R. Faulkner, Electrochemical Methods. Fundamentals and Applications, John Wiley & Sons, NY, 1980.
[39] Y.N. Gartstein, E.M. Conwell, Chem. Phys. Lett. 217 (1994) 41.